Neutron skin and isospin structure of giant resonances

H. Sagawa
Center for Mathematical Sciences, University of Aizu, Ikki-machi, Aizu-Wakamatsu, Fukushima 965-8580, Japan
(Received 25 December 2001; published 3 June 2002)

Neutron number dependence of neutron skin thickness in several isotopes is discussed by using Skyrme Hartree-Fock (HF) calculations. It is shown that the size of neutron skin is proportional to one-third power of the neutron number in all the isotopes studied although the central density varies substantially in each isotope. The isospin structure of giant quadrupole resonances (GQR) is also studied using self-consistent HF + random phase approximations. The isovector GQR is found to be a good isospin mode even in very neutron-rich nuclei, while the isoscalar GQR shows a large deviation from the pure isospin mode in neutron-rich C and O isotopes due to a strong neutron skin effect.

DOI: 10.1103/PhysRevC.65.064314 PACS number(s): 21.10.Pc, 21.60.Jz, 24.30.Cz

I. INTRODUCTION

The recent development of radioactive nuclear beams opens a new era to explore structure and reaction mechanism of nuclei near the drip lines. A unique feature of the neutron drip line nuclei is a large ratio of the neutron number to the proton number, which gives rise to the large difference in the the neutron and the proton Fermi energies in the single-particle potential. Namely, the neutron Fermi energy becomes close to the threshold, while the proton one is very deep in the mean field potential. Particles in the neutron single-particle orbits near the threshold will extend their wave functions beyond the core of nucleus and form a neutron skin in the density profile. Experimental evidence of the neutron skin has been obtained recently in many neutron-rich nuclei from high energy heavy-ion reaction cross sections [1]. We will study the size of the neutron skin quantitatively in C, O, Ca, Ni, Sn, and Pb isotopes by Skyrme Hartree-Fock (HF) calculations.

The asymmetry of the two Fermi energies may change basic properties of excitation modes. An interesting problem is the validity of the isospin classification of the excitation mode, i.e., whether the terms of isoscalar (IS) and isovector (IV) modes are valid or not for labeling the collective excitations in the neutron drip line nuclei [2–4]. We will study this problem by looking at giant quadrupole resonances (GQR) in β-stable and drip line nuclei of C, O, and Ca isotopes. The main purpose of this paper is twofold. We study the neutron number dependence of the size of neutron skin and its effect on the isospin structure of GQR.

As a theoretical model, we adopt HF calculations for the ground states and a HF+random phase approximation (RPA) theory for the excited states with the use of Skyrme interactions [5,6]. In the RPA calculations, we take into account proton and neutron degrees of freedom simultaneously with the coupling to the continuum solving the Green's function in the coordinate space. No assumption is made for the isospin structure of GQR. We use the SIII interaction as an effective interaction for HF and RPA calculations. We check the interaction dependence with another Skyrme interaction SkM*. Section II is devoted to neutron skin problems in the HF calculations. Since detailed descriptions of the present HF+RPA model is given elsewhere [2,6], the model is briefly discussed in Sec. II. RPA results are analyzed in comparison with the harmonic vibration mode in Sec. III. Conclusions are given in Sec. IV.

II. NEUTRON SKIN IN HF POTENTIAL

In Fig. 1, the neutron and proton HF potentials with the SIII interaction are shown in ^{12}C, ^{16}C, and ^{20}C together with the single-particle energies of ^{20}C. The HF calculations are performed by using the filling approximation, in which particles occupy the single-particle orbits from the bottom of the potential in order. The neutron potentials in the right panel of Fig. 1 show similar radial dependence in the three nuclei, while the proton ones become deeper and wider in heavier C isotopes. These results are caused by the dominant proton-neutron interaction in the HF field. It is also seen that the neutron Fermi energy in ^{20}C is about 25 MeV higher that the

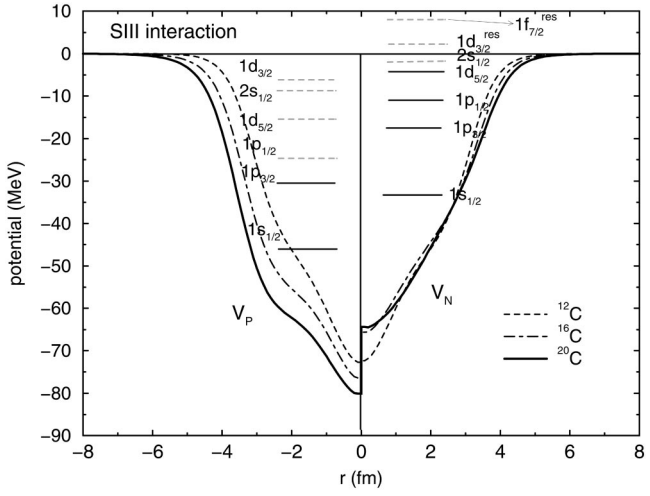

FIG. 1. Hartree-Fock potentials of ^{12}C, ^{16}C, and ^{20}C and single-particle energy levels in ^{20}C. V_N(r) on the right-hand side are the neutron nuclear potentials, while V_P(r) on the left-hand side are the proton nuclear potentials, respectively. The notation $(nl_j)^{\mathrm{res}}$ denotes the calculated single-particle resonant level in the HF potential. Occupied levels are indicated by full lines, while unoccupied levels are shown by broken lines. The SIII interaction is used for the HF calculations of all nuclei.

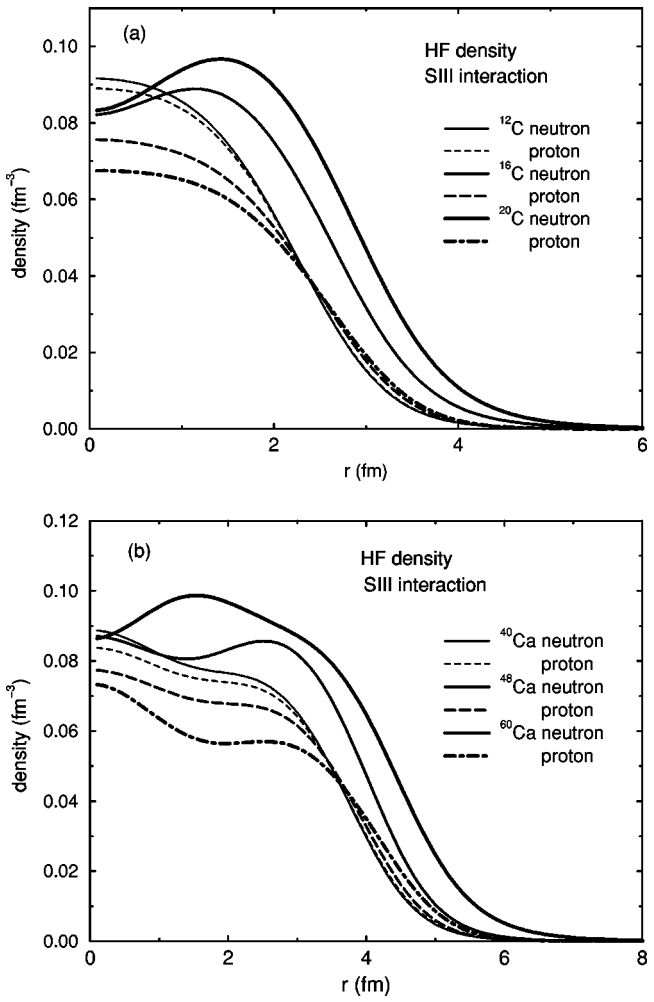

FIG. 2. HF densities of protons and neutrons. (a) $^{12}_{6}C_6$, $^{16}_{6}C_{10}$, and $^{20}_{6}C_{14}$ and (b) $^{40}_{20}Ca_{20}$, $^{48}_{20}Ca_{28}$, and $^{60}_{20}Ca_{40}$. The SIII interaction is used.

proton one and close to the threshold energy. The large asymmetries in the HF results are also found in other isotopes near the drip lines [7].

The HF proton and neutron densities are shown in Fig. 2(a) for C isotopes and Fig. 2(b) for Ca isotopes. Although the central density varies substantially in each isotope, the increase of the radius $r_{1/2}$ at around half central density $\rho = 0.045$ fm^{-3} is very regular: 2.25(2.21), 2.71(2.67), and 3.04(3.02) fm for ^{12}C, ^{16}C, and ^{20}C, respectively, and 3.29(3.23), 3.63(3.56), 4.05(4.01), and 4.48(4.46) fm for ^{34}Ca, ^{40}Ca, ^{48}Ca, and ^{60}Ca, respectively, with the SIII (SkM*) interaction. The increase of the radius $r_{1/2}$ is expressed by the relation

$$r_{1/2} \approx (N/N_{(\mathrm{core})})^{1/3} r_{1/2(\mathrm{core})}, \qquad (1)$$

where $N(N_{(\mathrm{core})})$ is the neutron number of nucleus (the core). The cores are ^{12}C for C isotopes and ^{40}Ca for Ca isotopes. There is essentially no interaction dependence on the relation (1). It is seen in Fig. 2 that the proton densities of heavier isotopes show a leaking effect in the tail region due to wider proton potential widths [8]. Consequently, the central parts of

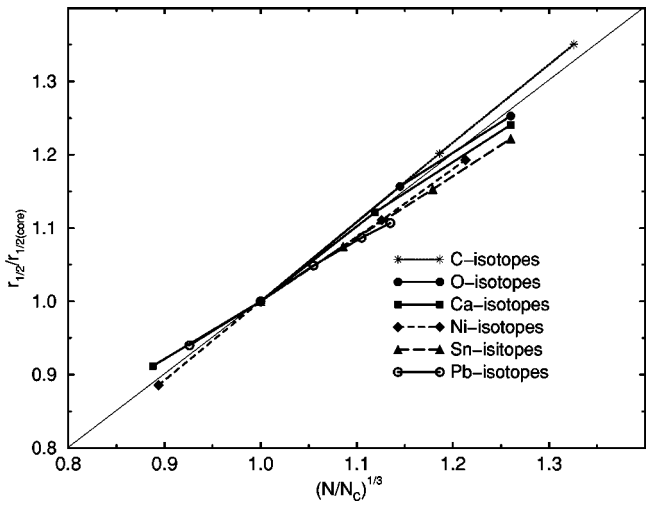

FIG. 3. The proportionality between $r_{1/2}/r_{1/2(\mathrm{core})}$ values and $(N/N_{(\mathrm{core})})^{1/3}$ in C, O, Ca, Ni, Sn, and Pb isotopes. The core neutron numbers $N_{(\mathrm{core})}$ are taken to be 6, 8, 20, 28, 50, and 82 for C, O, Ca, Ni, Sn, and Pb isotopes, respectively. The radius $r_{1/2}$ is calculated at the neutron density $\rho_n = 0.045$ fm^{-3}.

proton densities are decreasing largely in heavier isotopes. The neutron skin in Fig. 2(b) also increases for heavier Ca isotopes following the relation (1). The central part of the neutron density at around $r = 1.5$ fm in ^{60}Ca is much larger than those of ^{40}Ca and ^{48}Ca since the $2p_{3/2}$ and $2p_{1/2}$ orbits are occupied in ^{60}Ca and these wave functions have large components in the central part of the nucleus. A large leaking of the proton density is also seen in the tail region in ^{60}Ca due to the wider proton potential.

We extend the study of the relation (1) for other O, Ni, Sn, and Pb isotopes in the case of SIII interaction. The results are summarized in Fig. 3. As is seen in Fig. 3, the proportional relation holds in all the isotopes within an accuracy of less than 3%. It is interesting to notice that a neutron-rich C isotope ^{20}C shows a slightly larger $r_{1/2}/r_{1/2(\mathrm{core})}$ value than the $(N/N_{(\mathrm{core})})^{1/3}$ one, while the heavier neutron-rich Ca, Ni, Sn, and Pb nuclei have somewhat smaller $r_{1/2}/r_{1/2(\mathrm{core})}$ values than the corresponding $(N/N_{(\mathrm{core})})^{1/3}$ ones.

III. GIANT QUADRUPOLE RESONANCES AND NEUTRON SKIN EFFECT

In Sec. II, we pointed out a growth of thick neutron skin in neutron-rich C, O, and Ca isotopes. We will study in this session how the neutron skin affects on giant resonances (GR) by using the self-consistent HF+RPA model. GQR is selected as a typical mode of collective vibration. In order to calculate GQR strength, the RPA Green's function $G_{\mathrm{RPA}}(\mathbf{r},\mathbf{r}';E)$ is obtained in the coordinate space using the SIII interaction. The RPA strength function is then obtained by [2,6]

$$S(E) \equiv \sum_n |\langle n|\hat{O}(\lambda=2)|0\rangle|^2 \delta(E-E_n)$$

$$= \frac{1}{\pi} \mathrm{Im\,Tr}[\hat{O}(\lambda=2)^{\dagger} G_{\mathrm{RPA}}(E) \hat{O}(\lambda=2)], \qquad (2)$$

where $\hat{O}(\lambda=2)$ expresses one-body operators

$$\hat{O}(\lambda=2,\tau=0)=\sum_{i=1}^{A} r_i^2 Y_{2\mu}(\hat{r}_i)$$

for the isoscalar quadrupole response, (3)

$$\hat{O}(\lambda=2,\tau=1)=\sum_{i=1}^{A} \tau_z r_i^2 Y_{2\mu}(\hat{r}_i)$$

for the isovector quadrupole response, (4)

$$\hat{O}(E2)=\sum_{i=1}^{Z} r_i^2 Y_{2\mu}(\hat{r}_i)$$

for the charge quadrupole response. (5)

The IS, IV, and electric quadrupole responses in ^{20}C to the fields (3), (4), and (5) are shown in Fig. 4(a). The IS GQR peak is found at Ex=21.3 MeV with a large width due to the coupling to the continuum. The summed strength in the energy region 10 MeV$\leqslant$Ex$\leqslant$25 MeV exhausts 73% of the IS EWSR value. Since the low energy strength below Ex=15 MeV is governed by continuum neutron excitations, except a sharp peak at Ex=5.8 MeV, the IS and IV responses have almost the same strength in this energy region and the charge response is much quenched in the IS GQR region. The IV strength below the IS GQR peak is very large in ^{20}C because of large strength from the single-particle neutron orbits near the Fermi energy. In Fig. 5, the unperturbed strengths from three neutron orbits $1d_{5/2}$, $1p_{1/2}$, and $1p_{3/2}$ are shown together with the total unperturbed and IS RPA strengths. The last occupied neutron orbit in ^{20}C is $1d_{5/2}$ so that the $(2s_{1/2},1d_{5/2}^{-1})$ and $(1d_{3/2}^{\rm res},\ 1d_{5/2}^{-1})$ configurations are available in the low-energy region near the threshold. The unperturbed particle-hole (p-h) excitation $(2s_{1/2},1d_{5/2}^{-1})$ appears at Ex=1.8 MeV as a discrete state which is not drawn in Fig. 4(a). The peaks in the unperturbed strength at around Ex=7 and 25 MeV are due to the excitations $(1d_{3/2}^{\rm res},1d_{5/2}^{-1})$ and $(1f_{7/2}^{\rm res},\ 1p_{3/2})$, respectively. Because of a small neutron separation energy $S(n)=3.87$ MeV of the $1d_{5/2}$ orbit, the continuum $(s_{1/2},1d_{5/2}^{-1})$ excitation dominates the unperturbed transition strength up to 20 MeV. The neutron strength in Fig. 5 remains large near the IS GQR energy when the RPA correlations are taken into account. This is because of weak RPA correlations on the threshold strength. Two main IV peaks are found in ^{20}C at around Ex=32 and 40 MeV in Fig. 4(a). The summed strength 30 MeV$\leqslant$Ex$\leqslant$60 MeV exhausts 55% of the IV EWSR. The charge response above Ex=30 MeV is substantial, while IS strength is very small. These features are essentially the same in the results of another interaction SkM*.

The RPA results of ^{60}Ca are shown in Fig. 4(b). The IS GQR peak is seen at Ex=15.6 MeV exhausting 84% for 12 MeV$<$Ex$<$18 MeV of the EWSR with a width of about

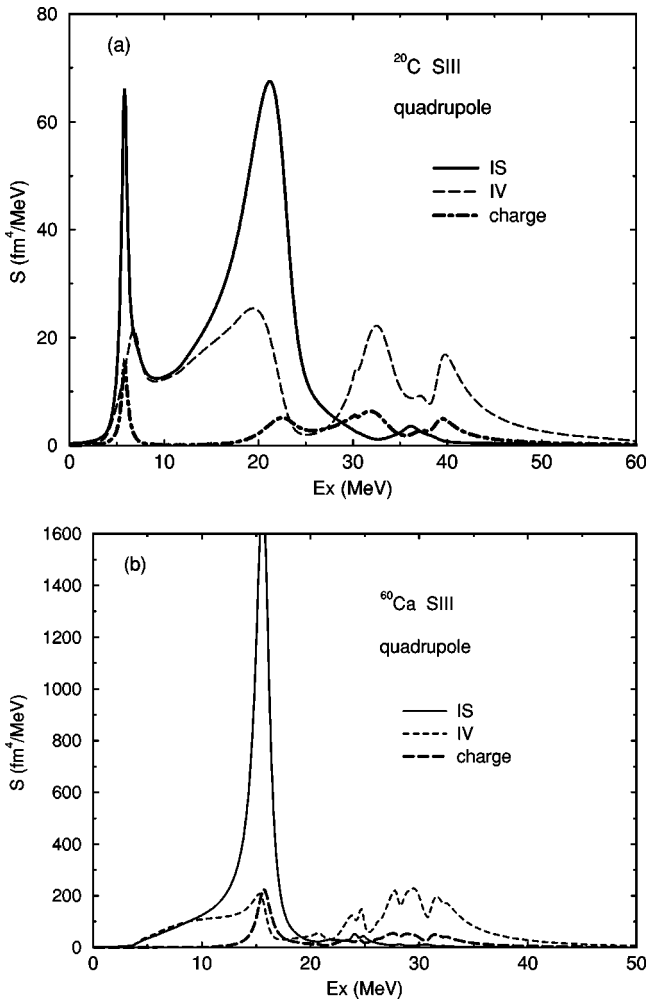

FIG. 4. The RPA strength functions for the IS, IV, and the charge quadrupole mode as a function of excitation energy. (a) $^{20}_{6}C_{14}$ and (b) $^{60}_{20}Ca_{40}$. The transitions operators (3), (4), and (5) are used for the calculations of the IS, IV, and the charge quadrupole response, respectively. The strength function $S(E)$ is averaged with a Lorenzian weighting function with a width $\Gamma=0.5$ MeV as a guide for eyes. The SIII interaction is used consistently in HF and RPA calculations.

1.0 MeV. Due to the large orbital angular momentum ($l=3$) for the least bound $1f_{5/2}$ neutrons, the IS and IV quadrupole response in ^{60}Ca increase gradually from the neutron threshold of 3.6 MeV with almost equal magnitudes and then merge into the IS GQR. The IV strength accompanying the IS GQR is the results of neutron excess in the IS mode. The IV GQR is very much fragmented in the energy region 20 MeV$<$Ex$<$40 MeV because of the large Landau damping effect exhausting 69% of the EWSR. Although the IV GQR is spread in the wide energy region, the charge response is always seen below in this high-energy region.

In order to clarify quantitatively the isospin structure of GQR, we introduce the harmonic vibration model by Bohr and Mottelson [9] to compare with the present RPA results. In the harmonic vibration model, the collective vibrational modes are described in terms of the variations in the mean field potential produced by an oscillation in the nuclear den-

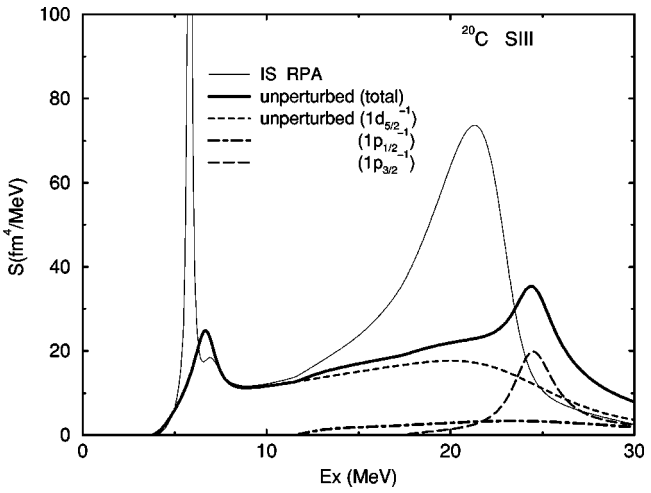

FIG. 5. The unperturbed and IS RPA strength of quadrupole transitions in $^{20}_{6}C_{14}$. The unperturbed strength from the orbits $1d_{5/2}$, $1p_{1/2}$, and $1p_{3/2}$ are shown by dashed, dot-dashed, and long-dashed curves, respectively, while the total unperturbed strength is drawn by a thick solid line. The IS RPA strength is given by a thin solid line. The SIII interaction is used.

sity. For small amplitudes of oscillation, the variation can be written in the form

$$\delta V = \kappa \alpha \hat{F}, \tag{6}$$

where κ and α are the coupling constant and the collective amplitude, respectively, while $\hat{F}$ is the vibrational field characterized by the multipolarity, the isospin, and the spin. Let us denote the collective one phonon state as $|n=1\rangle$. The zero-point amplitude for $|n=1\rangle$ is given by

$$\alpha_0 \equiv \langle n=1|\hat{F}|\hat{0}\rangle. \tag{7}$$

The effect of the neutron excess on the collective modes is given by the normal modes based on the assumption that the isospin structure of these modes is determined by the strong proton-neutron force in the nucleus. In the IS mode ($\tau=0$), the neutron-proton force will preserve the local ratio of neutrons and protons so that the mode is excited by the operator which acts symmetrically on protons and neutrons

$$\hat{F}^{\lambda}_{\tau=0} = \sum_{i=1}^{A} r_i^{\lambda} Y_{\lambda,\mu}(\hat{r}_i) = \sum_{i=1}^{N} r_i^{\lambda} Y_{\lambda,\mu}(\hat{r}_i) + \sum_{i=1}^{Z} r_i^{\lambda} Y_{\lambda,\mu}(\hat{r}_i) \equiv \hat{F}^{\lambda}_{\nu} + \hat{F}^{\lambda}_{\pi}. \tag{8}$$

The field of the IV mode acts on the difference of the isospin from its mean value

$$\hat{F}^{\lambda}_{\tau=1} = \sum_{i=1}^{A} \left(\tau_{zi} - \frac{1}{A} \sum_{i=1}^{A} \langle \tau_{zi} \rangle \right) r_i^{\lambda} Y_{\lambda,\mu}(\hat{r}_i) = \frac{2Z}{A} \hat{F}^{\lambda}_{\nu} - \frac{2N}{A} \hat{F}^{\lambda}_{\pi}. \tag{9}$$

For the dipole mode $\lambda=1$, Eq. (9) is equivalent to the subtraction of the center of mass spurious motion. In general cases $\lambda \neq 1$, it is the requirement that the field polarizes the neutron density against the proton density , but does not act on the total density at any point. Notice that the IS transition operator $\hat{O}(\mathrm{IS},\lambda=2)$ in Eq. (3) is the same as the IS field operator (8) with $\lambda=2$, while the IV transition operator $\hat{O}(\mathrm{IV},\lambda=2)$ in Eq. (4) is different to the IV operator (9) with $\lambda=2$.

We now look at separate proton and neutron contributions in the normal mode $|n=1\rangle$. Decomposing the IS mode ($\tau=0$) to the neutron and the proton parts

$$|(n=1,\tau=0)\rangle = |(n=1,\tau=0)\nu\rangle + |(n=1,\tau=0)\pi\rangle, \tag{10}$$

the zero-point amplitudes are given by

$$\alpha_0^{\tau=0,\nu} \equiv \langle (n=1,\tau=0)\nu|\hat{F}_{\nu}|\hat{0}\rangle = \langle (n=1,\tau=0)\nu|\hat{F}_{\tau=0}|\hat{0}\rangle \approx \frac{N}{A}\langle (n=1,\tau=0)|\hat{F}_{\tau=0}|\hat{0}\rangle, \tag{11}$$

$$\alpha_0^{\tau=0,\pi} \equiv \langle (n=1,\tau=0)\pi|\hat{F}_{\pi}|\hat{0}\rangle = \langle (n=1,\tau=0)\pi|\hat{F}_{\tau=0}|\hat{0}\rangle \approx \frac{Z}{A}\langle (n=1,\tau=0)|\hat{F}_{\tau=0}|\hat{0}\rangle. \tag{12}$$

In the last step of driving Eqs. (11) and (12), we adopt the approximate constant ratio of neutron to proton densities in the IS vibrational mode. The zero-point amplitudes (11) and (12) give the energy weighted sum rule (EWSR) [9]

$$\hbar\omega(\alpha_0^{\tau=0,\nu})^2 = \frac{\hbar^2}{2m}\frac{\lambda(2\lambda+1)}{4\pi}\frac{N^2}{A}\langle r^{2\lambda-2}\rangle, \tag{13}$$

$$\hbar\omega(\alpha_0^{\tau=0,\pi})^2 = \frac{\hbar^2}{2m}\frac{\lambda(2\lambda+1)}{4\pi}\frac{Z^2}{A}\langle r^{2\lambda-2}\rangle, \tag{14}$$

where $\hbar\omega$ is the energy of the normal mode. For the IS normal mode, we obtain a relation between the charge and IS strengths by using Eq. (12),

$$B(E\lambda,\tau=0) = \frac{Z^2}{A^2}B(\mathrm{IS},\tau=0). \tag{15}$$

The IV transition strength to the IS normal mode is finite in ($N \neq Z$) nuclei,

$$B(\mathrm{IV},\tau=0) = \frac{(N-Z)^2}{A^2}B(\mathrm{IS},\tau=0) \tag{16}$$

from Eqs. (11) and (12). The factors $(N/Z)^2$ for IS mode and $(1/2)^2$ for IV mode was pointed out for the core polarization charges for $E2$ transitions in Ref. [9].

The IV mode will be decomposed as

$$|(n=1,\tau=1)\rangle = |(n=1,\tau=1)\,\nu\rangle - |(n=1,\tau=1)\,\pi\rangle, \tag{17}$$

where the minus sign of the second term in the right-hand side reflects the polarization of neutrons against protons in the $(\tau=1)$ mode. The zero-point amplitudes for protons and neutrons in Eq. (17) are evaluated to be

$$\begin{aligned}\alpha_0^{\tau=1,\nu} &\equiv \langle (n=1,\tau=1)\,\nu|\hat{F}_\nu|\hat{0}\rangle \\ &= \frac{A}{2Z}\langle (n=1,\tau=1)\,\nu|\hat{F}_{\tau=1}|\hat{0}\rangle \\ &\approx \frac{A}{2Z}\frac{Z}{A}\langle (n=1,\tau=1)|\hat{F}_{\tau=1}|\hat{0}\rangle \\ &= \frac{1}{2}\langle (n=1,\tau=1)|\hat{F}_{\tau=1}|\hat{0}\rangle, \end{aligned} \tag{18}$$

$$\begin{aligned}\alpha_0^{\tau=1,\pi} &\equiv \langle (n=1,\tau=1)\,\pi|\hat{F}_\pi|\hat{0}\rangle \\ &= -\frac{A}{2N}\langle (n=1,\tau=1)\,\pi|\hat{F}_{\tau=1}|\hat{0}\rangle \\ &\approx -\frac{A}{2N}\frac{N}{A}\langle (n=1,\tau=1)|\hat{F}_{\tau=1}|\hat{0}\rangle \\ &= -\frac{1}{2}\langle (n=1,\tau=1)|\hat{F}_{\tau=1}|\hat{0}\rangle. \end{aligned} \tag{19}$$

In Eqs. (18) and (19), the proton and the neutron components in the $(\tau=1)$ mode is obtained assuming the total density invariance in the IV normal mode. We can evaluate the relations between the $E\lambda$ and IV strengths, and that between IS and IV strengths in the $(\tau=1)$ mode by using the amplitudes (18) and (19) to be

$$B(E\lambda,\tau=1) = \frac{1}{4}B(\mathrm{IV},\tau=1) \tag{20}$$

and

$$B(\mathrm{IS},\tau=1) = 0. \tag{21}$$

The zero IS strength in the $(\tau=1)$ mode is a direct consequence of the assumption of total density invariance in Eq. (9).

Ratios of integrated $E2$ to IS strengths of C, O, and Ca isotopes are shown in Fig. 6 in unit of $(Z/A)^2$ as a function of $(A/Z)^2$, while ratios of integrated $E2$ to IV strengths are shown in Fig. 7 in unit of $(1/2)^2$. The two Skyrme interactions SIII and SkM* are used to see the interaction dependence. The units $(Z/A)^2$ and $(1/2)^2$ are obtained in Eqs. (15) and (20) for the IS and IV normal modes , respectively. The RPA strengths are integrated in the IS and IV GQR energy regions to calculate the ratios in Figs. 6 and 7. In Fig. 7, the ratios in C, O, and Ca isotopes are close to unity and show

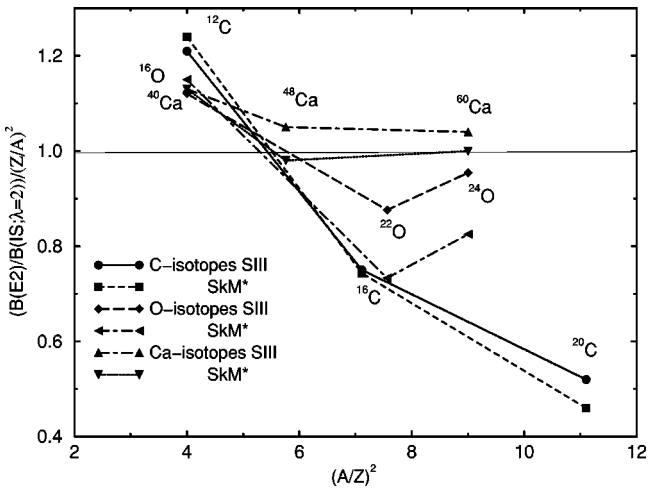

FIG. 6. Ratios of integrated charge strength $B(E2)$ to IS strength $B(\mathrm{IS},\lambda=2)$ in units of $(Z/A)^2$ near IS GQR of C, O, and Ca isotopes. The transition strength of IS peak of each C isotope is obtained by the integration with the energy interval of 6 MeV in $^{12}_{6}C_6$, 10 MeV in $^{16}_{6}C_{10}$, and 15 MeV in $^{20}_{6}C_{14}$ around the peak in the two interactions SIII and SkM*. In O isotopes, the integration intervals are 17 MeV$<$Ex$<$24 MeV (15 MeV$<$Ex$<$22 MeV) for $^{16}_{8}O_8$, 16 MeV$<$Ex$<$24 MeV (15 MeV$<$Ex$<$22.7 MeV) for $^{22}_{8}O_{14}$, and 13 MeV$<$Ex$<$24 MeV (12 MeV$<$Ex$<$22.8 MeV) for $^{24}_{8}O_{16}$, in the case of SIII (SkM*) interaction. In Ca isotopes, the integration intervals are 13 MeV$<$Ex$<$20 MeV (14 MeV$<$Ex $<$18.5 MeV) for $^{40}_{20}Ca_{20}$, 15 MeV$<$Ex$<$20 MeV (14 MeV$<$Ex$<$18 MeV) for $^{48}_{20}Ca_{28}$, and 12 MeV$<$Ex$<$18 MeV (12 MeV$<$Ex$<$17.5 MeV) for $^{60}_{20}Ca_{40}$ in the case of SIII (SkM*) interaction. The calculated RPA results except shown in Fig. 4 are taken from Refs. [6,10,11].

no appreciable (A/Z) dependence. These results suggest that the IV GQR is a good isospin mode in which the neutrons oscillate against the protons, preserving the total density invariance at any local point. While the results of SkM* in Fig. 7 gives a few % larger $B(E2)$ values for the IV GQR region in term of $B(IV)$, the interaction dependence is very small.

The ratios of $E2$ to IS strength in Fig. 6 show strong (A/Z) dependence in large C and O isotopes. Especially, the proton contribution in IS GQR is very much quenched in ^{20}C and ^{22}O even in unit of $(Z/A)^2$ due to a strong neutron skin effect. One can see also a small (A/Z) dependence in Ca isotopes. These results show that the assumption of the constant ratio of protons to neutrons in the $(\tau=0)$ mode is strongly violated in neutron-rich C isotopes, while this assumption is approximately valid in Ca isotopes. This difference depends strongly on available neutron configurations near the Fermi surface for the GQR. In ^{20}C and ^{22}O, the last occupied neutron orbit is $1d_{5/2}$ so that the continuum $(s_{1/2},1d_{5/2}^{-1})$ excitation dominates the low-energy region above the threshold up to 25 MeV as is seen in Fig. 5. The continuum neutron strength remains very large near the IS GQR energy even when the RPA correlations are taken into account. On the other hand, in ^{60}Ca, the last neutron $1f_{5/2}$ orbit has a larger angular momentum and available p-h configurations are much higher in energy for $\lambda=2$ excitations.

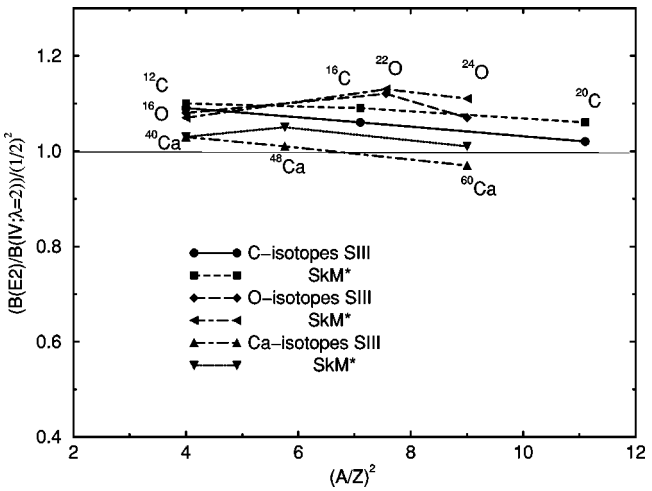

FIG. 7. Ratios of integrated charge strength $B(E2)$ to IV strength $B(\mathrm{IV},\lambda=2)$ in units of $(1/2)^2$ in the IV GQR region of C, O, and Ca isotopes. The strength in the IV GQR region of each C isotope is obtained by the integration of the energy interval 31 MeV<Ex<50 MeV (29 MeV<Ex<50 MeV) for $^{12}_{6}C_6$, 30.5 MeV<Ex<60 MeV (28.5 MeV<Ex<60 MeV) for $^{16}_{6}C_{10}$, and 30.5 MeV<Ex<60 MeV (29.0 MeV<Ex<60 MeV) for $^{20}_{6}C_{14}$ in the case of SIII (SkM*) interaction. In O isotopes, the integration intervals are 26 MeV<Ex<50 MeV (24 MeV<Ex<50 MeV) for $^{16}_{8}O_8$, 25 MeV<Ex<50 MeV (25 MeV<Ex<50 MeV) for $^{22}_{8}O_{14}$, and 25.7 MeV<Ex<50 MeV (23.2 MeV<Ex<50 MeV) for $^{24}_{8}O_{16}$, in the case of SIII (SkM*) interaction. The strength in the IV GQR region of each Ca isotope is obtained by the integration of the energy interval, 25 MeV<Ex<50 MeV (23 MeV<Ex<50 MeV) for $^{40}_{20}Ca_{20}$, 24.5 MeV<Ex<45 MeV (20 MeV<Ex<45 MeV) for $^{48}_{20}Ca_{28}$, and 20 MeV<Ex<40 MeV (20 MeV<Ex<40 MeV) for $^{60}_{20}Ca_{40}$ in the case of SIII (SkM*) interaction. The calculated RPA results except shown in Fig. 4 are taken from Refs. [6,10,11].

Thus the neutron skin configurations do not influence strongly on the isospin structure of GQR in ^{60}Ca. The results in Figs. 6 and 7 are essentially the same in the two Skyrme interactions SIII and SkM*.

The $B(E2)$ values in $N=Z$ nuclei are 10–20 % larger than the corresponding $B(IS)/(1/2)^2$ values in Fig. 6. The enhancement of $B(E2)$ compared to the harmonic vibration model is due to the Coulomb potential in the mean field, which makes lower the proton threshold energy than the neutron one. Consequently, in $N=Z$ nuclei, the proton contribution is somewhat larger than the neutron one in the IS GQR region.

In the heavier isotopes, the quenching effect on $B(E2)$ is more pronounced in the case of SkM* than that of SIII in Fig. 6 . The asymmetry energy coefficient a_τ is 26.1 and 28.2 MeV for SkM* and SIII, respectively. Because of the larger a_τ for SIII, the neutron threshold is smaller for SIII than that for SkM* in $N>Z$ nuclei. For example, the neutron separation energy $S(n)$ is 3.87 MeV for SIII and 4.86 MeV for SkM*. Thus, the threshold effect for the response function is stronger for SIII and absorbs larger neutron strength near the threshold, which is much lower in energy than the IS GQR. On the contrary, the threshold effect is relatively weak in SkM* and the neutron skin effect remains to be large in the IS GQR region and gives the larger quenching of the $B(E2)$ value for SkM* than that of SIII in the neutron-rich nuclei in Fig. 6.

The change of the isospin structure affects the core polarization charges in nuclei near the neutron drip line since the proton amplitudes of GR play the decisive role to determine the magnitude of the polarization charges. It is pointed out that the small proton amplitudes of IS GQR in neutron-rich C isotopes give a large quenching of the proton polarization charges [10]. Recent experimental data of Q moments in B isotopes confirm the quenching of the polarization charges [12]. The ratio of the proton to neutron amplitudes is also crucial to analyze experimental cross sections by proton scatterings and Coulomb excitations in neutron-rich nuclei to obtain the $B(E2)$ transition strength [13]. Thus, the character of isospin mode should be carefully examined with microscopic models.

IV. SUMMARY

We discussed the neutron number dependence of neutron skin thickness in the C, O, Ca, Ni, Sn, and Pb isotopes by using the HF results. It is pointed out in the six isotopes that the neutron skin radius shows a fairly good proportionality to one-third power of the neutron number although the central densities vary substantially in different isotopes . The leaking of proton density is seen in the surface region of the neutron-rich isotopes due to the wider proton potentials. The isospin structure of the GQR is also studied in the framework of the self-consistent HF+RPA model in comparison with the harmonic vibrational model. It is found that IV GQR behaves as a good isospin mode although the transition strength is spread in a wide energy region. This feature of the IV GQR is also obtained by looking at the IS strength in the IV GQR energy region in Refs. [2,3]. On the other hand, the IS GQR is very much affected by the neutron skin effect, especially in the neutron-rich C and O isotopes and shows a large deviation from the pure isospin mode in the harmonic vibration model. The IV strength under the IS GQR was studied in ^{28}O and ^{48}Ca by using the same HF+RPA model in Ref. [2] and the strong effect of the neutron excess on the isospin structure of IS GQR was pointed out. In this paper, the neutron skin effect on the IS GQR was clarified more quantitatively and systematically in C, O, and Ca isotopes.

ACKNOWLEDGMENTS

I would like to thank I. Hamamoto, M. Ishihara, and I. Tanihata for enlightening discussions. This work was supported in part by the Japanese Ministry of Education, Science, Sports and Culture by a Grant-In-Aid for Scientific Research under Program No. C(2) 12640284.

[1] A. Ozawa, T. Suzuki, and I. Tanihata, Nucl. Phys. **A693**, 32 (2001).
[2] I. Hamamoto, H. Sagawa, and X.Z. Zhang, Phys. Rev. C **55**, 2361 (1997); J. Phys. G **24**, 1417 (1998).
[3] F. Catara, E.G. Lanza, M.A. Nagarajan, and A. Vitturi, Nucl. Phys. **A614**, 86 (1997).
[4] I. Hamamoto, Phys. Rev. C **60**, 031303(R) (1999).
[5] I. Hamamoto and H. Sagawa, Phys. Rev. C **54**, 2369 (1996).
[6] I. Hamamoto, H. Sagawa, and X.Z. Zhang, Nucl. Phys. **A626**, 669 (1997).
[7] I. Hamamoto and H. Sagawa, Phys. Rev. C **64**, 024313 (2001).
[8] J. Dobaczewski, I. Hamamoto, W. Nazarewicz, and A. Sheik, Acta Phys. Pol. B **25**, 541 (1994).
[9] A. Bohr and B.R. Mottelson, *Nuclear Structure* (Benjamin, Reading, MA, 1975), Vol. II, Chap. 6.
[10] H. Sagawa and K. Asai, Phys. Rev. C **63**, 064310 (2001).
[11] H. Sagawa (unpublished).
[12] H. Izumi *et al.*, Phys. Lett. B **366**, 51 (1996); H. Ogawa *et al.*, *ibid.* **451**, 11 (1999); H. Ogawa *et al.* (unpublished).
[13] H. Iwasaki *et al.*, Phys. Lett. B **481**, 7 (2000); P.G. Thirolf *et al.*, *ibid.* **485**, 16 (2000); E. Khan *et al.*, *ibid.* **490**, 45 (2000).